

Rare and challenging extra-axial brain lesions: CT and MRI findings with clinico-radiological differential diagnosis and pathological correlation

Mustafa Kemal Demir, Özlem Yapıcıer, Elif Onat, Zafer Orkun Toktaş, Akın Akakın, Kamran Urgun, Türker Kılıç

ABSTRACT

There are many kinds of extra-axial brain tumors and tumor-like lesions, and definitive diagnosis is complicated in some cases. In this pictorial essay, we present rare and challenging extra-axial brain lesions including neuroenteric cyst, primary leptomeningeal melanomatosis, isolated dural neurosarcooidosis, intradiploic epidermoid cyst, ruptured dermoid cyst, intraventricular cavernoma, and cavernous hemangioma of the skull with imaging findings and clinico-radiological differential diagnosis, including the pathologic correlation. Familiarity with these entities may improve diagnostic accuracy and patient management.

Intracranial extra-axial pathologies arise from tissues other than brain parenchyma, such as meninges, dura, calvarium, ventricles, choroid plexus, pineal gland, or pituitary gland. There are many kinds of extra-axial tumors and tumor-like lesions, and their definitive diagnosis can often be made easily via imaging studies. However, conditions such as rarity, atypical localization or overlapping symptomatology may complicate the diagnosis.

In this pictorial essay, we present a few examples of rare and challenging extra-axial brain lesions from our archive with a brief review of clinico-radiological differential diagnosis, including the pathologic correlation. It should be noted that there are many other rare extra-axial brain lesions that are not mentioned in this text, such as solitary fibrous tumor, hemangiopericytoma, leiomyosarcoma, plasmacytoma, Rosai-Dorfman disease, and inflammatory myofibroblastic tumor.

Neuroenteric cyst

Neuroenteric cysts are very rare congenital malformative endodermal lesions. The midline of the posterior fossa anterior to the brainstem or craniocervical junction is the classic location of the intracranial disease. However, they can be seen in the cerebellopontine angle, fourth ventricle, and even supratentorially. Headache is the most common clinical symptom. Dizziness, focal neurological signs such as impairments of 3th 5th and 8th nerves, or seizures may also be seen. Computed tomography (CT) and magnetic resonance imaging (MRI) appearances of the cyst may be variable depending on protein content. They may be isodense, hypodense, or hyperdense on CT scans. Since most of them are proteinaceous, they are usually hyperintense on T1-weighted and hypointense on T2-weighted MR sequences. The lesions show no restricted diffusion on diffusion-weighted imaging (DWI). On contrast-enhanced imaging studies they may rarely show rim enhancement. The differential diagnosis of the disease may include epidermoid cysts, dermoid cysts, arachnoid cysts, Rathke's cleft cysts, and colloid cysts. Ventral displacement of the basilar artery away from the brainstem pial surface is a recently described unique imaging finding for the disease in classic location and would lead to a prompt radiological diagnosis (Fig. 1a–1d) (1).

The histomorphological appearance of neuroenteric cysts reveals a lining epithelium that ranges from nonciliated to ciliated, cuboidal to columnar, with a variable number of Goblet cells (Fig. 1e). However, Rathke's cleft cysts and colloid cysts share identical findings with them, suggesting a common endodermal origin.

From the Departments of Radiology (M.K.D. ✉ demir.m.k@gmail.com), Pathology (Ö.Y., E.O.) and Neurosurgery (Z.O.T., A.A., K.U., T.K.), Bahçeşehir University School of Medicine, Goztepe Medical Park Hospital, Istanbul/ Turkey.

Received 31 January 2014; revision requested 2 March 2014; final revision received 12 March 2014; accepted 18 March 2014.

Published online 19 June 2014.
DOI 10.5152/dir.2014.14031

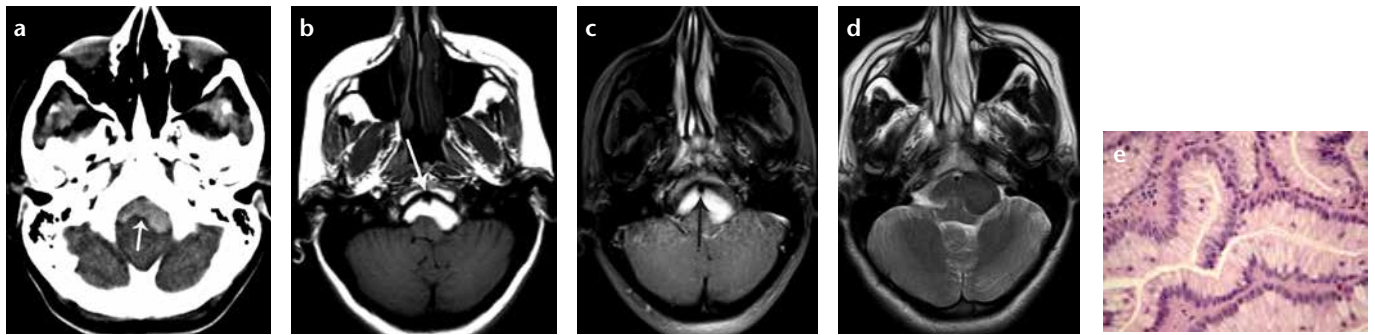


Figure 1. a–e. Neuroenteric cyst in a 28-year-old female patient with headache. Axial unenhanced CT scan (a) shows a well-defined oval hyperdense midline mass anterior to the brainstem (arrow). There is no bony abnormality. The cyst is hyperintense to brain parenchyma and cerebrospinal fluid on axial T1-weighted MR images without (b) and with fat saturation (c). The cyst is hypointense on axial T2-weighted MR image (d). There is ventral displacement of the basilar artery away from the brainstem pial surface which is a unique imaging finding for the disease in this classic location (b, arrow). Photomicrograph (e) shows the cyst lined by columnar mucinous epithelium (original magnification, $\times 400$; hematoxylin-eosin [H-E] stain).

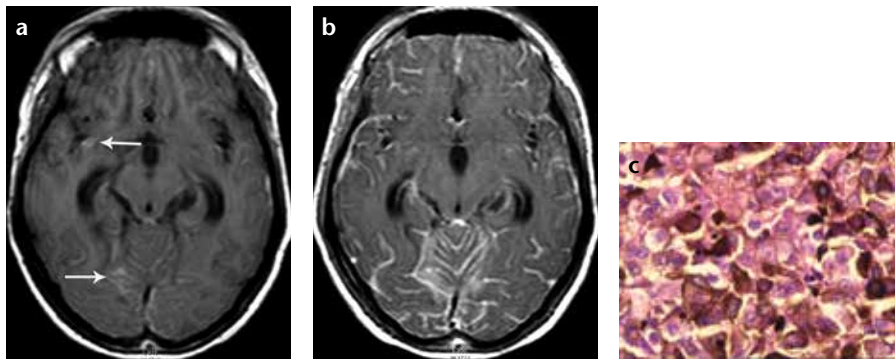


Figure 2. a–c. Primary leptomeningeal melanomatosis in an 18-year-old male patient with progressive headache, nausea, vomiting, and learning disabilities. Axial unenhanced T1-weighted MR image (a) demonstrates hydrocephalus associated with high signal intensities in the cisterns and sulci of the brain (arrows), and axial contrast-enhanced T1-weighted MR image (b) demonstrates intense and irregular leptomeningeal enhancement. Photomicrograph (c) demonstrates uniform sheets of epithelioid cells with regular nuclear profiles exhibiting prominent nucleoli. Mitotic activity was inconspicuous and necrosis was absent but dusty pigmentation was seen throughout the lesion (original magnification, $\times 400$; H-E stain).

Primary leptomeningeal melanomatosis

Primary leptomeningeal melanomatosis (PLM) is a very rare and aggressive neoplasm. It originates from leptomeningeal melanocytes in the pia arachnoid of the base of the brain, caudal medulla, or cervical spinal cord. Clinical symptoms may vary, and patients may present with seizures, psychiatric disturbances, cranial nerve palsies, or signs of increased intracranial pressure—including headache, vomiting, papilla edema, and deterioration of consciousness. The antemortem diagnosis of the disease depends on the presence of leptomeningeal malignant infiltration and hydrocephalus without any primary tumor in or outside the central nervous system, and positive ventricular or lumbar cerebrospinal fluid cytology. The most important MRI clue in the diagnosis of the disease

is the identification of the high signal intensities in the subarachnoid spaces of the brain and/or spinal cord on unenhanced T1-weighted images due to melanin. Diffuse irregular intense contrast enhancement of the subarachnoid spaces without any parenchymal involvement is another important diagnostic clue of the PLM (Fig. 2a, 2b) (2, 3). Accumulation of malignant cells in the subarachnoid spaces usually results in hydrocephalus. The main differential diagnosis of PLM includes malignant primary or metastatic neoplasms of the leptomeninges, proteinaceous aggressive infections, granulomatous diseases, or idiopathic hypertrophic cranial pachymeningitis.

Microscopically, tumor cells reveal vesicular nuclei with prominent nucleoli and dusty cytoplasmic pigment. S-100, vimentin, and HMB45 immu-

nopositivity is diagnostic for malignant melanoma, as well as immunonegativity for glial fibrillary acid protein or cytokeratins (Fig. 2c).

Isolated dural neurosarcoidosis

Sarcoidosis is an idiopathic systemic granulomatous disease characterized by the presence of noncaseating granulomas in various tissues. Less than 1% of patients have isolated central nervous system involvement. The posterior fossa is the most common site, followed by the frontobasal and temporal regions. Patients with dural neurosarcoidosis typically present with headaches or cranial nerve compression. Cranial nerve involvement in sarcoidosis may occur along with meningeal thickening besides nerve compression. MRI reveals dural thickening which is hypointense on T2-weighted images. The lesions show prominent homogeneous enhancement on contrast-enhanced T1-weighted images. Imaging abnormalities may resolve after medical therapy (Fig. 3a–3c). Although very useful in suggesting the diagnosis, T2 hypointensity is not specific for dural neurosarcoidosis and may also be seen in calcified meningiomas, dural metastases, lymphomas, Wegener granulomatosis, and rheumatoid nodules (4). Presence of adjacent bone changes, mostly hyperostosis is of high diagnostic value in differentiation of meningioma from isolated dural mass of sarcoidosis. MRI and clinical findings can serve as a key to the diagnosis of dural neurosarcoidosis.

The typical microscopic finding of dural sarcoidosis includes noncaseating granulomas consisting of macrophages,

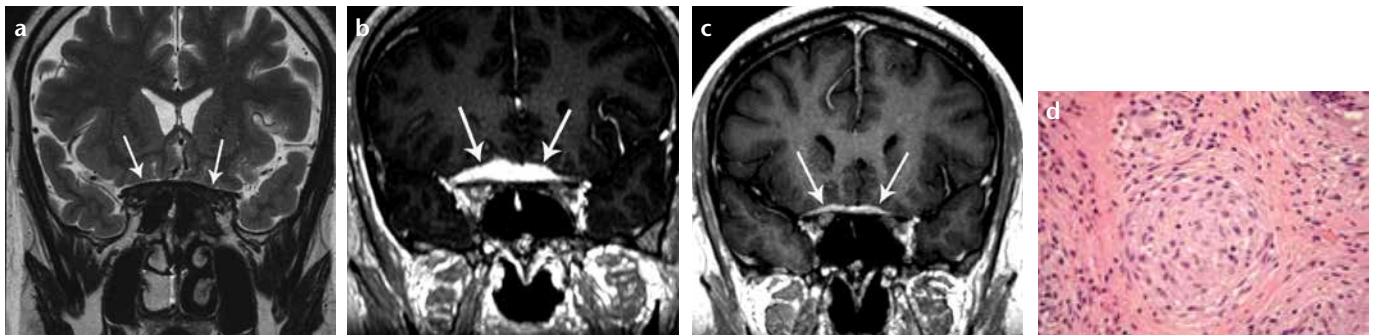


Figure 3. a–d. Dural sarcoidosis (*arrows*) in a 38-year-old male patient. Coronal T2-weighted MR image (**a**) shows marked T2-hypointensity of frontobasal dural thickening characteristic of sarcoidosis. Contrast-enhanced coronal T1-weighted MR image (**b**) shows frontobasal dural thickening and enhancement. The follow-up contrast-enhanced coronal T1-weighted MR image after corticosteroid treatment (**c**) demonstrates marked improvement confirming the diagnosis. Photomicrograph (**d**) shows dural noncaseating granulomatous inflammation (original magnification, $\times 400$; H-E stain).

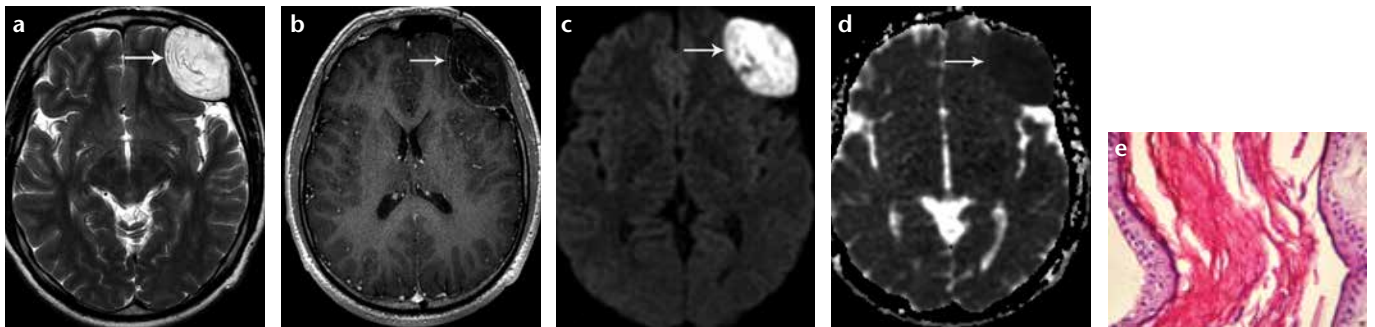


Figure 4. a–e. Intradiploic epidermoid tumor (*arrow*) in a 35-year-old male patient with headache and painless left frontal swelling under the scalp. Axial T2-weighted MR image (**a**) demonstrates an inhomogeneous hyperintense lesion in the left frontal intradiploic space. Axial post-gadolinium T1-weighted MR image (**b**) shows no prominent enhancement of the inhomogeneous hypointense lesion. Diffusion-weighted image (**c**) shows the lesion to be brightly hyperintense. The ADC map (**d**) shows that the diffusion abnormality is due to restriction and not a T2-shine-through phenomenon. Photomicrograph (**e**) shows the cyst with keratinized squamous epithelial lining, filled with keratin (original magnification, $\times 400$; H-E stain).

macrophage-derived epithelioid cells, and multinucleated giant cells (Fig. 3d). However, a variety of other granulomatous conditions must be excluded before the diagnosis of sarcoidosis, since noncaseating granulomatous inflammation is not specific for sarcoidosis.

Intradiploic epidermoid cyst

Intradiploic epidermoid cysts are derived from the ectodermal cells of the cranium and are lined solely by stratified squamous epithelium. They are extremely rare; common locations include the occipital, frontal, and parietal bones. Since these cysts grow very slowly, the onset of symptoms and signs is often late, over a period of months to years. These lesions usually present as painless bony swelling under the scalp. They may cause headaches due to erosion of the calvarium, and seizures due to local pressure. These cysts may perforate the dura, rupture into the subarachnoid space with resulting chemical meningitis, or involve the brain

parenchyma. They are hypoattenuating lesions on CT scans. MR images reveal inhomogeneous hypointense T1 signal and inhomogeneous hyperintense T2-FLAIR signal intensities. Lesions typically do not enhance. When present, contrast enhancement is minimal and peripheral. DWI is the best imaging sequence in diagnosing epidermoid cysts. They show restricted diffusion with higher signal intensity than that of cerebrospinal fluid on DWI. Differential diagnosis may include sebaceous cyst, dermoid cyst, hematoma with fibrosis, lipoma, and fibroma (5, 6). MRI findings in the presence of DWI, is usually specific for the final radiological diagnosis (Fig. 4a–4d).

Microscopically the wall of the cystic tumor is lined by squamous epithelium and the cyst is filled with lamellated keratin content (Fig. 4e).

Ruptured dermoid cyst

Intracranial dermoid cysts are non-neoplastic congenital ectodermal

inclusion cysts containing apocrine, sweat, and sebaceous cysts, as well as hair follicles, squamous epithelium, and teeth. Histomorphological appearance consists of cutaneous-type epithelium with hair follicles and sebaceous glands. When the cyst is ruptured foreign-body giant cells and inflammation are seen. They tend to occur in the midline more frequently than epidermoids. The clinical presentation of the disease is quite variable. Headache and seizure are the most common symptoms. Dermoid cysts appear as well defined lobulated heterogeneous hypoattenuating masses with negative Hounsfield units due to their rich lipid content on CT scans. Calcifications may be present. Enhancement is uncommon. On MRI, they are heterogeneous hyperintense on T1-weighted sequences and show a variable signal, from hypo- to hyperintensity on T2-weighted sequences. They usually demonstrate high signal intensity on DWI and FLAIR sequences. When a dermoid tumor ruptures into

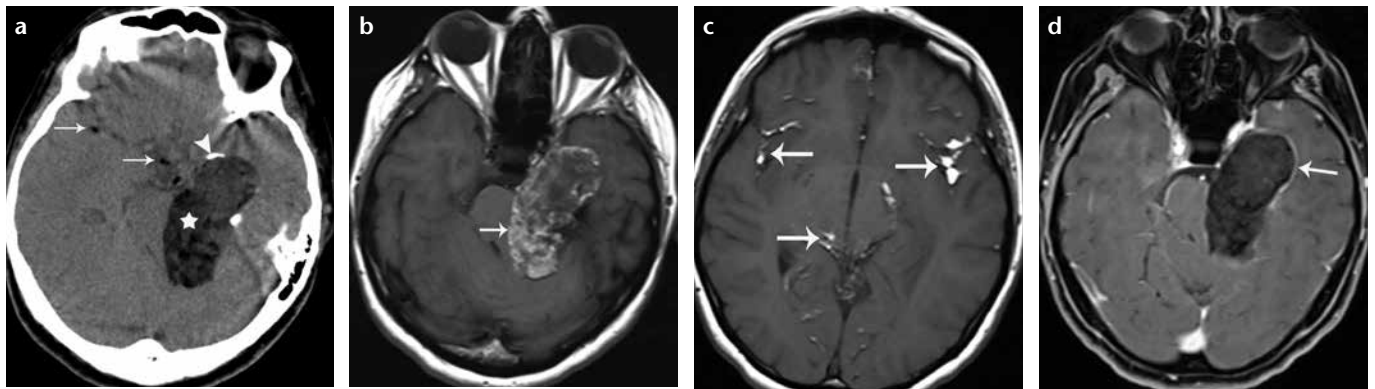


Figure 5. a–d. Ruptured dermoid cyst in a 39-year-old female patient with headache and loss of consciousness. Unenhanced axial brain CT image (a) shows a heterogeneous fat attenuation in an off-midline extra-axial mass (*star*) anteromedial to the left petrous bone extending to the middle and posterior cranial fossae. Calcification is seen in the cyst wall (*arrowhead*). There are fat droplets in the subarachnoid space due to rupture (*arrows*). The lesion shows heterogeneous hyperintense areas on T1-weighted MR image (b) due to fat content (*arrow*). Scattered foci of hyperintense fat droplets are seen throughout the subarachnoid space on T1-weighted MR image (c, *arrows*). Fat-suppressed contrast-enhanced T1-weighted MR image (d) shows loss of hyperintense signal intensity of the mass compatible with a fat containing lesion and peripheral rim enhancement (*arrow*).

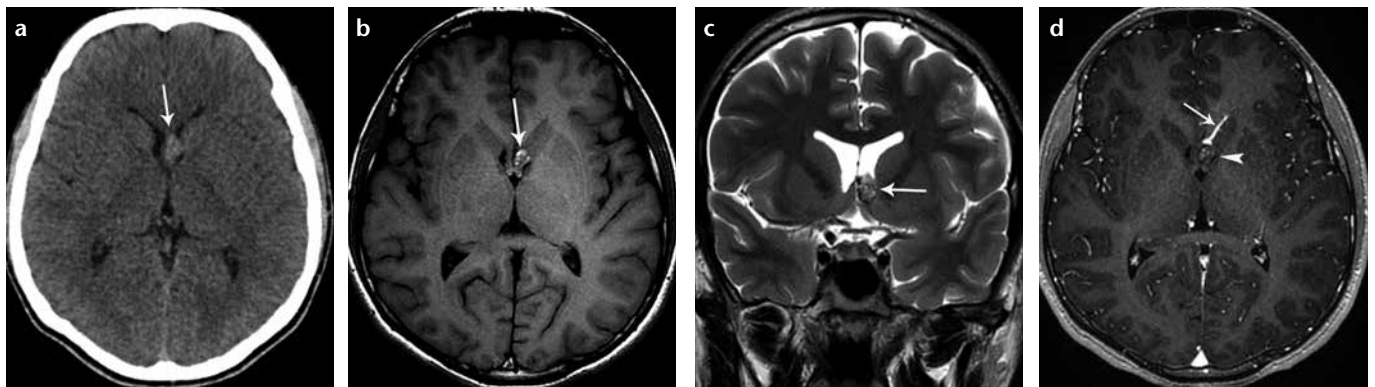


Figure 6. a–d. Intraventricular cavernoma as an incidental finding in an 18-year-old male patient. Axial CT scan (a) shows an oval, well-circumscribed, hyperdense mass lesion in the left frontal horn of lateral ventricle (*arrow*). The lesion shows heterogeneous hyperintense and hypointense signals on axial T1-weighted MR image (b, *arrow*). There is a typical peripheral hemosiderin rim of low signal intensity on coronal T2-weighted MR image (c, *arrow*). There is no enhancement on contrast-enhanced axial MR image (d, *arrowhead*), but an enhancing parenchymal venous angioma is seen in front of the intraventricular cavernoma (d, *arrow*).

the ventricles and subarachnoid and/or subdural spaces, fat droplets appear as hypodense on CT or hyperintense on MRI (Fig. 5). Chemical meningitis may lead to vasospasm, infarction, hydrocephalus, and even death (7). If chemical meningitis exists, intense pial or ventricular ependymal enhancement may be seen on contrast-enhanced imaging studies. Epidermoids, teratomas, lipomas, craniopharyngiomas, and occasionally arachnoid cysts may be confused with dermoid cysts. Epidermoid cysts usually show diffusion restriction on DWI. Soft tissue components of teratomas enhance on postcontrast images. Lipomas show homogeneous fat attenuation and/or signal intensity. Craniopharyngiomas typically demonstrate calcification and generally have enhancement on contrast-enhanced images. The presence of solid enhancing nodules in the cyst wall

favors the diagnosis of craniopharyngioma. Arachnoid cysts have the same appearance as cerebrospinal fluid at all sequences (8, 9).

A review of CT and MR images usually allows the radiologists to make the correct preoperative diagnosis.

Intraventricular cavernoma

Cavernomas occur rarely in the ventricular system. They have a particular predisposition to bleeding. They may extend outside the ventricle wall to the intra-axial compartment. Clinical presentation depends on its location in the ventricles and the presence of bleeding. Most cavernomas are asymptomatic and are found incidentally. The disease may cause headache, nausea/vomiting, hydrocephalus, cranial nerve deficit, and hemiparesia depending on the location. The differential diagnosis of the intraventricular cavernoma may in-

clude any intraventricular tumor such as central neurocytoma, choroid plexus papilloma, meningioma, ependymoma, subependymal giant cell astrocytoma, and germinoma. Intraventricular cavernomas are hyperdense on unenhanced CT. Their appearance on MRI is usually characteristic. There are foci of hyperintensity on T1-weighted MR images due to various age of blood products (i.e., methemoglobin). T2 shortening producing a black halo around the lesion represents peripheral hemosiderin. Contrast enhancement may be associated with venous angioma (Fig. 6). They typically have no mass effect and surrounding vasogenic edema, unless complicated by significant hemorrhage (10).

Cavernous hemangioma of the skull

Cavernous hemangiomas of the skull are rare and most often locate in the

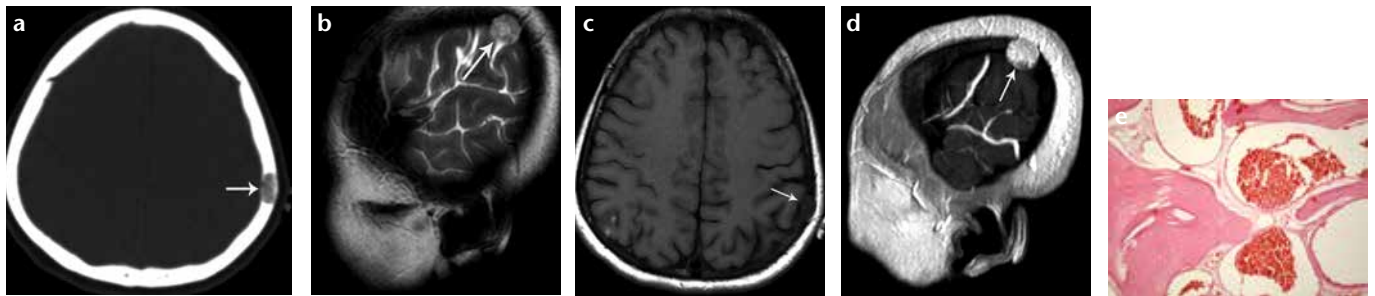


Figure 7. a–e. Cavernous hemangioma of the parietal bone (arrows) in a 37-year-old with headache. Axial CT scan (a) shows lytic, well-defined defect characterized by a fine, reticular pattern without a sclerotic rim involving both inner and outer tables. The lesion is heterogeneously hyperintense on sagittal T2-weighted MR image (b), and hypointense on axial T1-weighted MR image (c). Contrast-enhanced sagittal T1-weighted MR image (d) shows marked homogeneous enhancement. Photomicrograph (e) shows cavernous vascular lesion within the bone (original magnification, $\times 200$; H-E stain).

frontal and parietal bones. These tumors are slow growing and are generally asymptomatic. Clinical presentation may be a painless palpable scalp mass. It is a lytic, well-defined defect characterized by a fine, reticular pattern without a sclerotic rim, involving both inner and outer tables on CT scans. The MRI signal is variable depending on the amount of fat content (Fig. 7a–7d). The hyperintensity of hemangiomas at T1-weighted sequences is an important distinguishing feature for this tumor (11).

Microscopically, cavernous angiomas consist of sclerotic, variably calcified compact vessels in a honeycomb pattern (Fig. 7e). Unlike telangiectasis and arteriovenous malformation these lesions do not contain interstitial parenchyma.

Conclusion

We have briefly reviewed the imaging characteristics of rare pathologies of extra-axial brain compartment. Familiarity with these extra-axial brain lesions and increased awareness of their imaging findings and differential

diagnosis should improve the interpretation of the images, leading to reduced errors and increased diagnostic value in reporting.

Conflict of interest disclosure

The authors declared no conflicts of interest.

References

1. Uschold T, Xu DS, Wilson DA, et al. Diagnostic and surgical implications of ventral vertebrobasilar displacement by posterior fossa neurenteric cysts. *World Neurosurg* 2013 Oct 16. PII: S1878–8750(13)01362–4. DOI: 10.1016/j.wneu.2013.10.037. [Epub ahead of print] [\[CrossRef\]](#)
2. Smith AB, Rushing EJ, Smirniotopoulos JG. Pigmented lesions of the central nervous system: radiologic-pathologic correlation. *Radiographics* 2009; 29:1503–1524. [\[CrossRef\]](#)
3. Demir MK, Aker FV, Akinci O, Ozgültekin A. Case 134: Primary leptomeningeal melanomatosis. *Radiology* 2008; 247:905–909. [\[CrossRef\]](#)
4. Shah R, Roberson GH, Curé JK. Correlation of MR imaging findings and clinical manifestations in neurosarcoidosis. *AJNR Am J Neuroradiol* 2009; 30:953–961. [\[CrossRef\]](#)
5. Samdani S, Kalra GS, Rawat DS. Post-traumatic intradiploic epidermoid cyst of frontal bone. *J Craniofac Surg* 2013; 24:128–130. [\[CrossRef\]](#)
6. Hasturk AE, Basmaci M, Yilmaz ER, Kertmen H, Gurer B, Atilgan AO. Giant intradiploic epidermoid cyst presenting as solitary skull mass with intracranial extension. *J Craniofac Surg* 2013; 24:2169–2171. [\[CrossRef\]](#)
7. Karabulut N, Oguzkurt L. Tetra-ventricular hydrocephalus due to ruptured intracranial dermoid cyst. *Eur Radiol* 2000; 10:1810–1811. [\[CrossRef\]](#)
8. Osborn AG, Preece MT. Intracranial cysts: radiologic-pathologic correlation and imaging approach. *Radiology* 2006; 239:650–664.
9. Ray MJ, Barnett DW, Snipes GJ, Layton KF, Opatowsky MJ. Ruptured intracranial dermoid cyst. *Proc (Bayl Univ Med Cent)* 2012; 25:23–25. [\[CrossRef\]](#)
10. Kivelev J, Niemelä M, Kivisaari R, Hernesniemi J. Intraventricular cerebral cavernomas: a series of 12 patients and review of the literature. *J Neurosurg* 2010; 112:140–149. [\[CrossRef\]](#)
11. Xu P, Lan S, Liang Y, Xiao Q. Multiple cavernous hemangiomas of the skull with dural tail sign: a case report and literature review. *BMC Neurol* 2013; 13:155.